

## Ion Transport Mechanisms in Liquid-Liquid Interface

Baofu Qiao, John V. Muntean, Monica Olvera de la Cruz and Ross J. Ellis

### S1. Atomistic MD Simulation Methodology

#### S1.a. Simulation details

Classical MD simulations were performed at the all-atom resolution using the package GROMACS (version 4.5.5).<sup>1</sup> General AMBER Force Field (GAFF) was employed.<sup>2</sup> The TIP3P water model is used, as recommended by the AMBER force field.<sup>3</sup>

The missing atomic partial charges of cyclohexane, 1-pentanol and CTA<sup>+</sup> were calculated using Gaussian 09 package<sup>4</sup> following the recommended procedure of the restrained electrostatic potential (RESP) under GAFF.<sup>2</sup> They were optimized using the basis set of B3LYP/6-31G(d), followed by the single point energy calculation under HF/6-31G(d). The calculated atomic partial charges and the GAFF were justified by means of two simulations, which predicted the densities of pure cyclohexane and pentanol systems under ambient condition (298 K and 1 bar) of  $772 \pm 4 \text{ kg/m}^3$  and  $822 \pm 4 \text{ kg/m}^3$ , respectively, in good agreement with the corresponding experimental data of  $774 \text{ kg/m}^3$  and  $814.4 \text{ kg/m}^3$ . The force field parameters of Br<sup>-</sup> (i.e., the counterion of CTA<sup>+</sup>) are from Ref. [5], which has been optimized based on the TIP3P water model.

**Table S1.** Number of Different Components in the Systems Investigated<sup>a</sup>

	water	pentanol	[CTA] <sup>+</sup> •Br <sup>-</sup>	HDEHP	cyclohexane	Time /ns <sup>b</sup>
SYSTEM	2000	500	100	6	6000	100/280
Control	2000	500	100		6000	100/50

a) These numbers correspond to the experimental concentrations of 3 M for water, 0.75 M for pentanol, 0.15 M for [CTA]<sup>+</sup>•Br<sup>-</sup>, 0.009 M for HDEHP.

b) Simulation times in the annealing and production simulations.

Two different systems were simulated. In the main system, the extractant HDEHP is included, which is excluded in the control system. The numbers of the components are listed in **Table S1**. Such numbers are chosen so that the final system box length is roughly equal to 11 nm, which corresponds to the distance between neighbor reverse micelles experimentally observed (**Scheme 1d** in the main text). Moreover, the experimental concentrations of all the solute species are consistent with the corresponding experimental data.

All the initial structures for atomistic MD simulations were built by means of package Packmol.<sup>6</sup> To speed up the simulation on the self-assembly process, all the solute molecules were distributed within a smaller and central cubic box of 7 nm, which was surrounded by the solvent cyclohexane molecules in the simulation box with the initial edge length of 12 nm. Note the initial simulation box (12 nm) is a little large than the expected equilibrium box length of 11 nm, which is to easily accommodate all the molecules under Packmol. The initial and final structures of the ‘SYSTEM’ are provided below.

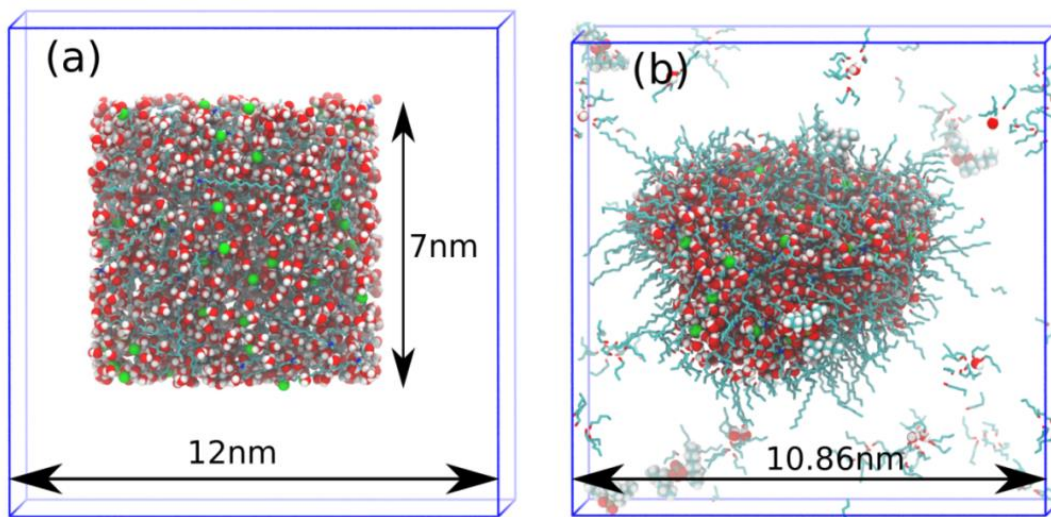


**Figure S1.** Snapshots of (a) the initial and (b) the final structures in the system ‘SYSTEM’. In (a), all the solute molecules are distributed in a cubic box of length of 7 nm, which is embedded in the cyclohexane box of the edge length of 12 nm initially. In both snapshots, the cyclohexane molecules (solvent) and the hydrogen atoms of pentanol and CTA<sup>+</sup> molecules are omitted for the display. The colors are the same as in the **Figure 2** in the main text.

The energy minimization was firstly performed using the steepest descent algorithm to equilibrate the systems. The annealing simulations were subsequently employed to speed up the aggregation process of solute molecules.<sup>7</sup> In the annealing process, the system temperature was elevated from 298 K to 363 K in 0.5 ns, stayed at 363 K for another 0.5 ns, and then decreased back to 298 K within 0.5 ns. It was subsequently maintained at 298 K for 3.5 ns. The annealing process was repeated 20 times. See **Table S1** for the annealing simulation time. During the annealing simulations, the isothermal-isobaric ensemble (NTP, constant number of particles, temperature and pressure) was used. The temperature was coupled via the velocity rescaling algorithm, with the pressure coupled via the Berendsen coupling (reference pressure 1 bar, characteristic time 1 ps, compressibility  $4.5 \times 10^{-5} \text{ bar}^{-1}$ ). The three-dimensional periodic boundary conditions were employed. The neighbor searching was performed up to the distance of 0.9 nm. The long-range coulomb interactions were calculated using the smooth Particle Mesh Ewald (PME) method<sup>8-9</sup> with a grid real spacing of 0.12 nm and the cubic interpolation. The van der Waals interactions were calculated up to a cutoff distance of 0.9 nm, in combination with the long-range dispersion correction for energy and pressure.

The production simulations were subsequently performed based on the corresponding structures of the last frames of the annealing simulations. In the production simulations, the temperature was coupled via the Nose-Hoover algorithm (reference temperature 298 K, characteristic time 0.5 ps) in combination with the pressure coupled by means of Parrinello-Rahman (reference pressure 1 bar, characteristic time 4 ps, compressibility  $4.5 \times 10^{-5} \text{ bar}^{-1}$ ). All the chemical bonds are constrained so that a large simulation integration time step of 2.5 fs was employed. The simulations were performed for a duration of up to 280 ns (**Table S1**). The simulation frames were saved at a frequency of 10 ps for data collection and analysis.

To justify the convergence of the simulations, we calculated the short-range (coulomb and Lennard-Jones) potential energies between water-oil (cyclohexane), water-surfactant (CTA<sup>+</sup>), water-cosurfactant (pentanol) and water-extractant (HDEHP), which are presented in **Figure S2**. All these energies are converged during the production simulation. Moreover, the negligible fluctuation in the density ( $808 \pm 1 \text{ kg/m}^3$ ) also supports the equilibration of the simulation.

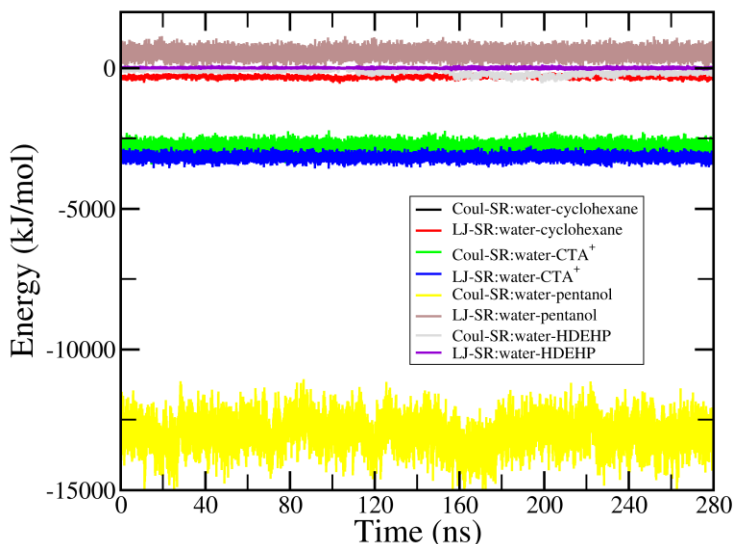


**Figure S2.** Potential energies between water-oil (cyclohexane), water-surfactant (CTA<sup>+</sup>), water-cosurfactant (pentanol), and water-extractant (HDEHP) in the production simulation of system SYSTEM, justifying the equilibration of the simulation.

### S1.b. Definition of center-of-mass of waters

In all the simulations, the majority of waters are forming one whole giant water pool. See **Table S2**. Therefore, all waters are included in the calculation of the center-of-mass, which is required for the calculation of radial density distribution.

**Table S2.** Probability (%) of Waters Forming Reverse Micelle <sup>a</sup>

system	SYSTEM	Control
%	98.0	97.8

- a) Waters are defined as one cluster when their oxygen atoms are closer than 3.5 Å from each other. 3.5 Å is the first minimum of the O-O radial distribution function.

### S1.c Uncertainties in the HDEHP surface activity calculations

Due to the limited amount of HDEHP molecules (6) we can simulate, the uncertainties in the HDEHP surface activity calculation can't be simply ignored. To this end, we calculated the radial density profiles of phosphorous atoms from HDEHP headgroup in different simulation periods of 0-70, 70-140, 140-210 and 210-280 ns, and the corresponding integral number of phosphorous atoms as a function of the distance to the water center-of-mass. These calculated data are presented in **Figure S3**. The number of HDEHPs adsorbed at the water pool surface increases from 0.1 (0-70 ns), to 0.3 (70-140 ns) and 2.5 (140-210 ns), and then drops to 1.9 (210-280 ns), with the average number of around 1.1 in the total simulation duration of 280 ns. Regardless of the uncertainties, it always holds true that the majority of the HDEHP molecules are dissolved in the organic environment, that is, HDEHP is mostly surface inactive.

Some simulation snapshots are provided in **Figure S4**. The adsorption and desorption of HDEHPs at the water pool surface are both observed within the simulation duration of 280 ns, supporting the kinetic feature of the surface activity of the HDEHP molecules.

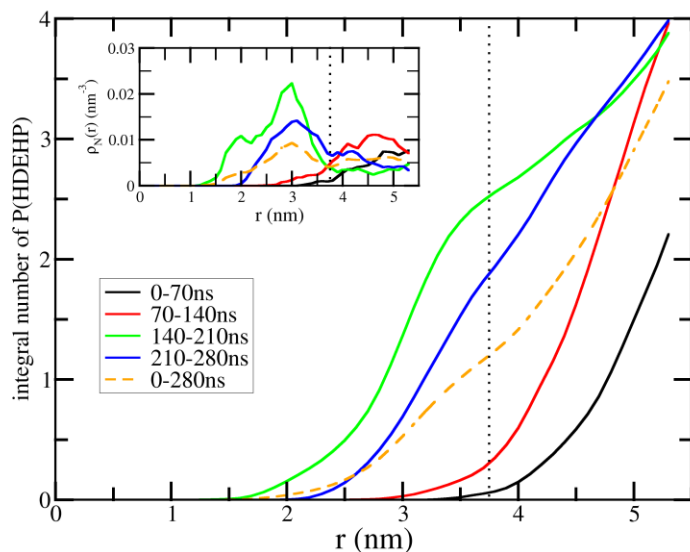


**Figure S3.** Integral number of phosphorous atoms from HDEHP as a function of the distance to the water center-of-mass in the different simulation time intervals. Insets are the corresponding radial density profiles. The vertical dotted lines refer to the cutoff distance (3.75 nm) of the adsorption layer, defined by the first minimum on the radial density profile in the time period of 0-280 ns (inset).

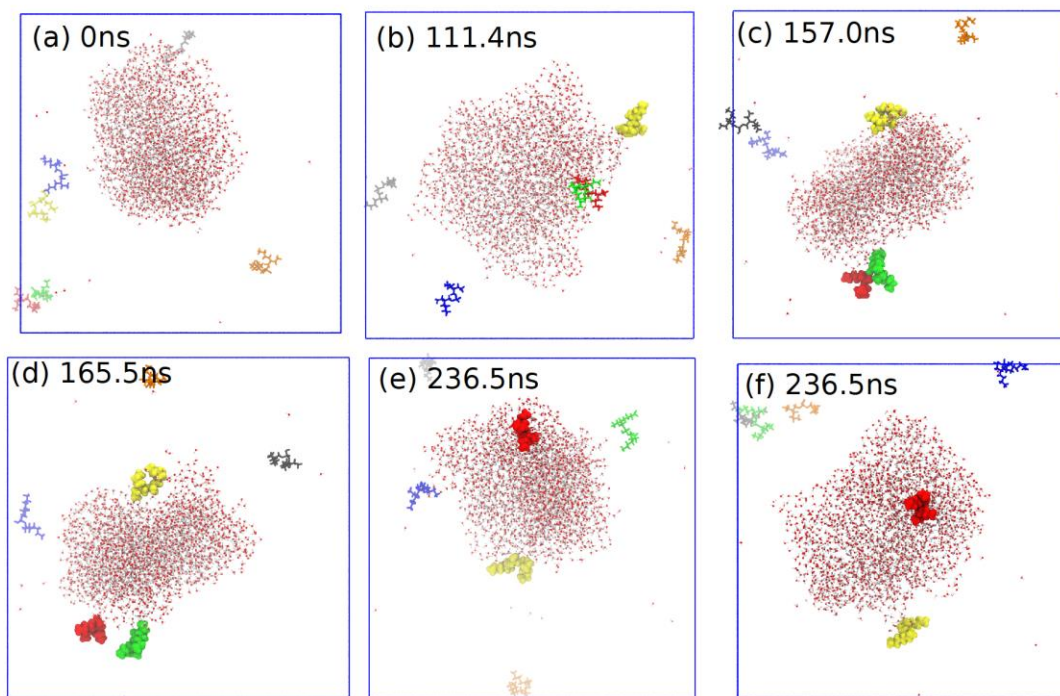


**Figure S4.** Snapshots of HDEHP molecule adsorption/desorption at the water pool surface. (a) At time of 0 ns of the production simulation, no HDEHP was adsorbed. Different colors are employed to represent different HDEHP molecules. (b) At 111.4 ns, one HDEHP (in yellow) was adsorbed. (c) At 157 ns, the HDEHP dimer (in red and green) was adsorbed, too. (d) At 165.5 ns, the HDEHP dimer (in red and green) broke apart. (e) At 236.5 ns, one HDEHP (green) was desorbed. (f) The final snapshot with 2 HDEPHs adsorbed (in red and yellow).

## S2. Microemulsion in the Absence of Extractant and $\text{Lu}(\text{NO}_3)_3$ Ion

When dissolved in oil, surfactants spontaneously assemble into reverse micelles around nanoscale pools of water to form water-in-oil microemulsions.<sup>10</sup> These thermodynamically stable oil dispersed aqueous domains can dissolve hydrophilic electrolytes (e.g., metal salts) to provide nano-confined ionic solutions.<sup>11-16</sup> When the water pool is voluminous enough, it behaves like bulk water,<sup>17-19</sup> so that the dissolved electrolytes are solvated in the same way as in a classical aqueous solution. In our study, a water-in-oil microemulsion was formulated to give reverse micelles large and numerous enough to provide a 5 nm diameter water pool in every  $(10 \text{ nm})^3$  unit volume, dimensions that are accessible to atomistic MD simulations. This was achieved by mixing water (3 M), cetyltrimethylammonium bromide (CTAB, 0.15 M) and 1-pentanol (0.75 M) in cyclohexane. CTAB was selected as the surfactant in this study because it is virtually insoluble as a free molecule in cyclohexane and so pertains exclusively at the oil/water interface in its ionized form. Under these conditions, CTAB stabilized reverse micelles of about 5 nm in diameter have previously been reported, with an area per CTAB headgroup of about  $60 \text{ \AA}^2$ ,<sup>20</sup> giving a total density of approximately one reverse micelle per  $(10 \text{ nm})^3$  volume in cyclohexane. In this way, a microemulsion was formulated that allows a single water droplet to be simulated using atomistic MD in an approx.  $(10 \text{ nm})^3$  box, with numbers of component molecules that reflect exactly the experimental conditions (Control in **Table S1**).

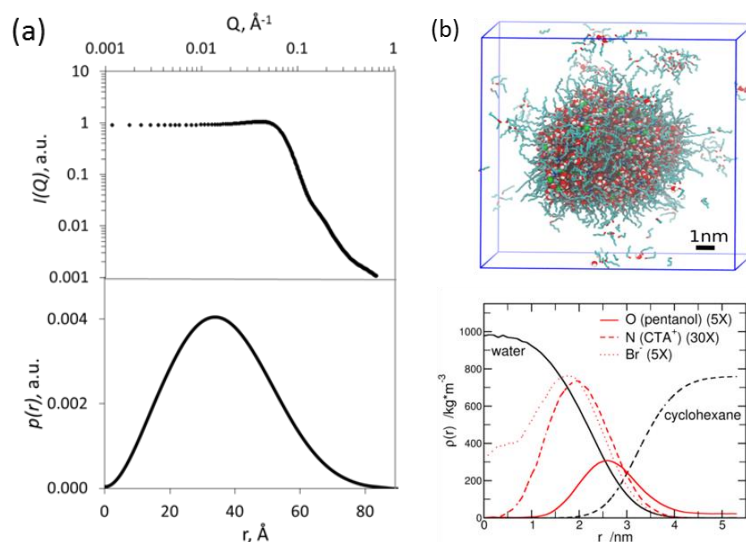


**Figure S5.** (a) Background-subtracted SAXS data (including solvent background) and corresponding GIFT-generated  $p(r)$  function of water-pentanol-CTAB-cyclohexane microemulsion; (b) Snapshot of the last frame in the simulation of the (water-pentanol-CTAB)-in-cyclohexane system (Control in Table S1) and the corresponding radial density distributions of all components. In the snapshot, O/N/Br/C/H is colored in red/blue/green/cyan/white, respectively using package VMD.<sup>21</sup> Note the hydrogen atoms of pentanol and CTA are omitted for the display, as well as cyclohexane molecules. The radial densities are calculated based on the center-of-mass of water molecules. The densities of pentanol oxygens,  $\text{CTA}^+$  nitrogen and  $\text{Br}^-$  atoms are magnified for the display.

The nanoscale structure of the microemulsion was characterized using small angle X-ray scattering (SAXS). SAXS is sensitive to the difference in electron density between the aqueous core and the surrounding hydrocarbon media (i.e., surfactant tails and solvent oil), and so holds information regarding the morphology of the water pool. The normalized, background-subtracted SAXS datum for the microemulsion shown in **Figure S5a** has a form that is typical for particle scattering (e.g., isolated water

globules in oil). However, the high concentration of particles causes interference from inter-particle scattering (i.e., structure factor) that is seen in the data as a broad peak at  $0.05 \text{ \AA}^{-1}$ . In order to determine the nanoscale structure of the water pools, the structure factor must be taken into account in treating the data, and this was achieved using the Generalized Indirect Fourier Transform (GIFT) method.<sup>22</sup> GIFT yields separate functions corresponding to structure factor (inter-particle scattering) and form factor (the scattering contribution from isolated particles) and generates a real space  $p(r)$  function that corresponds to the morphology of the scattering particle (i.e., the water pool) shown in **Figure S5a**. The bell-shaped character of the  $p(r)$  function indicates globular water pools of approximately spherical structure.<sup>23</sup> The maximum diameter of the aqueous globule is indicated by the maximum extent of the  $p(r)$  function along the x-axis at about  $80 \text{ \AA}$ , whereas the average diameter is estimated from the second inflection point of the  $p(r)$  function at  $52 \text{ \AA}$ .<sup>23</sup> These measurements were corroborated using dynamic light scattering (DLS) measurements giving a size distribution peak centered at  $68 \text{ \AA}$  (**Figure S6**), corresponding to the average diameter of the microemulsion droplet inclusive of the surfactant hydrocarbon chains. The minor oscillation in the experimental SAXS data at  $0.15 \text{ \AA}^{-1}$  corresponds to a correlation distance of  $42 \text{ \AA}$ . This feature may be generated from a shell of  $\text{Br}^-$  counterions, which has previously been reported in SAXS data from CTAB micelles in water.<sup>24</sup>

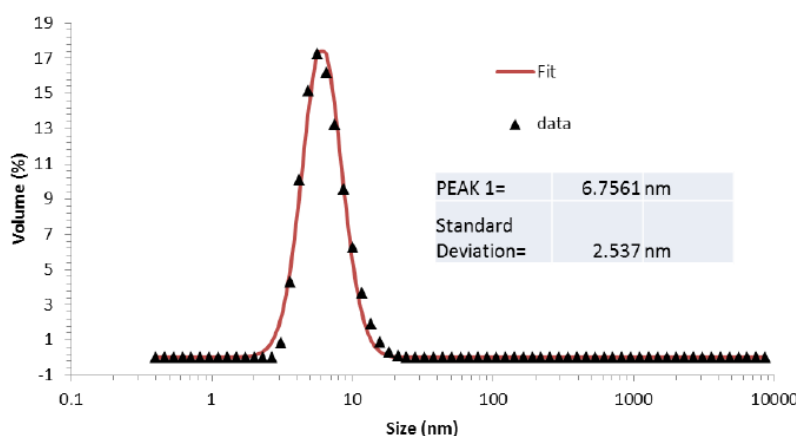


**Figure S6:** DLS results showing particle size of 6.8 nm.

The microemulsion was reproduced in an atomistic MD simulation by filling a box with the equilibrium length of approx. 11 nm and appropriate numbers of water, pentanol,  $\text{CTA}^+$ ,  $\text{Br}^-$  and cyclohexane molecules to reflect the experimental concentrations (solution Control in **Table S1**). After the equilibration of an annealing simulation, the production simulation run for 50 ns. The visualization of the simulation snapshot (**Figure S5b**) shows a single large globular reverse micelle, with the water molecules forming a core surrounded by a monolayer of  $\text{CTA}^+$  surfactant molecules that pertain exclusively on the interface. In comparison, the 1-pentanol molecules are only partially distributed at the water/cyclohexane interface. Radial density profiles of the component molecules were obtained throughout the simulation trajectory, taking the center-of-mass of the water core as the origin (**Figure S5**). The radial density profile for water has a maximum distance of about 3.8 nm, corresponding to a maximum aqueous core diameter of about  $76 \text{ \AA}$  (close to the maximum extent of the experimentally derived  $p(r)$  function in **Figure S5a**). The ‘average’ radius of the water-centered reverse micelle could be obtained as 2.85 nm based on the junction point of the density profiles of water and cyclohexane, close to the experimental measurement taken from the  $p(r)$  function of around 5.2 nm in diameter. The radial density profiles of water and cyclohexane overlap in the 2 - 4 nm region, which may be explained by the deformation of the globule from spherical symmetry (see, e.g., **Movie S1** in SI) and/or the penetration of water channel ‘fingers’ into the oil (see the main text). The  $\text{CTA}^+$  headgroups that make up the surfactant monolayer at the oil-water

interface has a radial density peak at 2.2 nm that also overlaps significantly with the tail of the water radial density profile. Most encouragingly, the radial density function for Br<sup>-</sup> has a peak at about 2 nm, which is consistent with the 42 Å distance corresponding to the correlation peak at 0.15 Å<sup>-1</sup> in the SAXS data assigned to the Br<sup>-</sup> shell. The convergent conclusions of reverse micelle structure derived from theory and experiment suggest that the water-in-oil microemulsion – formulated to give one nanoscale aqueous globule in a (10 nm)<sup>3</sup> volume of oil – has been well replicated in the atomistic MD simulation.

### Supporting Figures:

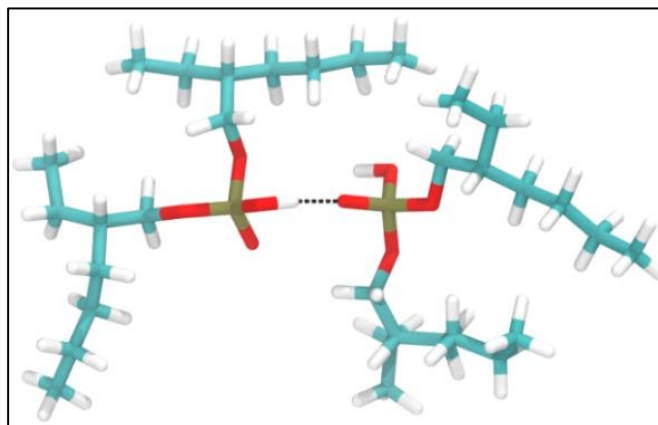


**Figure S7.** Snapshot of a HDEHP dimer in the system SYSTEM, which are interacting via H-bonds (black dotted line).

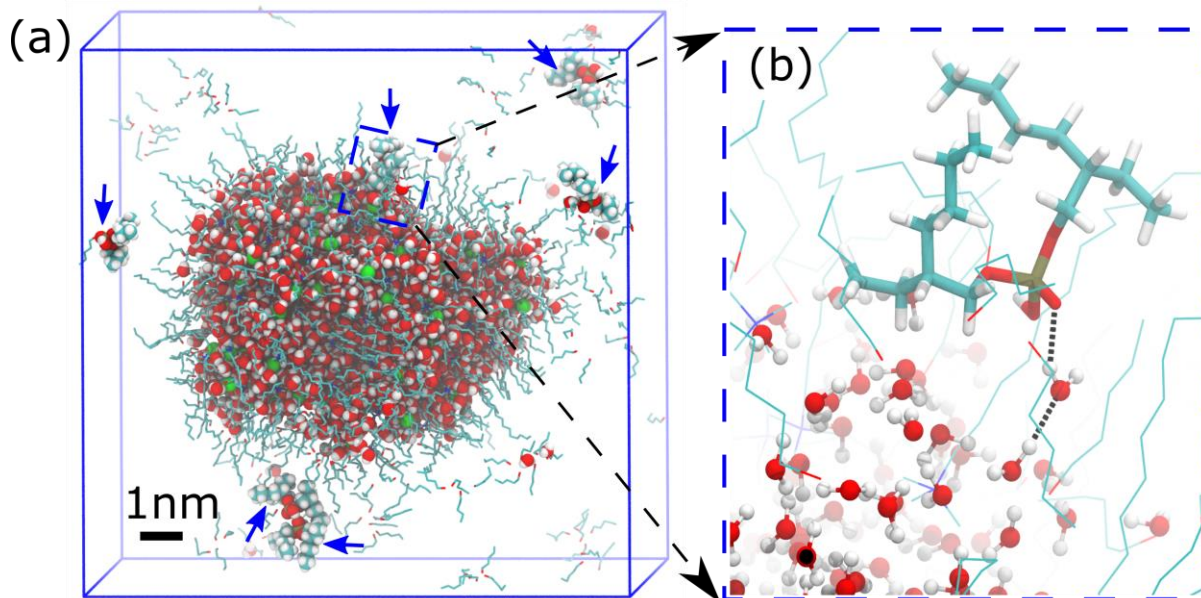


**Figure S8.** (a) Snapshots of the simulation frame illustrating the distribution of HDEHP (blue arrows). The solid blue lines refer to the boundary of the simulation boxes. In (b), the water-bridged H-bonding (dotted black lines) between HDEHP and water pool are highlighted.

### Supporting Movie:

**Movie S1.** A rotation movie of the simulation snapshot in **Figure 2a**.

## References:

1. Hess, B.; Kutzner, C.; van der Spoel, D.; Lindahl, E., GROMACS 4: Algorithms for Highly Efficient, Load-Balanced, and Scalable Molecular Simulation. *J. Chem. Theory Comput.* **2008**, *4*, 435-447.
2. Wang, J.; Wolf, R. M.; Caldwell, J. W.; Kollman, P. A.; Case, D. A., Development and testing of a general amber force field. *J. Comput. Chem.* **2004**, *25* (9), 1157-1174.
3. Sun, Y.; Kollman, P. A., Hydrophobic solvation of methane and nonbond parameters of the TIP3P water model. *J. Comput. Chem.* **1995**, *16* (9), 1164-1169.
4. Frisch, M. J.; Trucks, G. W.; Schlegel, H. B.; Scuseria, G. E.; Robb, M. A.; Cheeseman, J. R.; Scalmani, G.; Barone, V.; Mennucci, B.; Petersson, G. A.; Nakatsuji, H.; Caricato, M.; Li, X.; Hratchian, H. P.; Izmaylov, A. F.; Bloino, J.; Zheng, G.; Sonnenberg, J. L.; Hada, M.; Ehara, M.; Toyota, K.; Fukuda, R.; Hasegawa, J.; Ishida, M.; Nakajima, T.; Honda, Y.; Kitao, O.; Nakai, H.; Vreven, T.; Montgomery Jr., J. A.; Peralta, J. E.; Ogliaro, F.; Bearpark, M. J.; Heyd, J.; Brothers, E. N.; Kudin, K. N.; Staroverov, V. N.; Kobayashi, R.; Normand, J.; Raghavachari, K.; Rendell, A. P.; Burant, J. C.; Iyengar, S. S.; Tomasi, J.; Cossi, M.; Rega, N.; Millam, N. J.; Klene, M.; Knox, J. E.; Cross, J. B.; Bakken, V.; Adamo, C.; Jaramillo, J.; Gomperts, R.; Stratmann, R. E.; Yazyev, O.; Austin, A. J.; Cammi, R.; Pomelli, C.; Ochterski, J. W.; Martin, R. L.; Morokuma, K.; Zakrzewski, V. G.; Voth, G. A.; Salvador, P.; Dannenberg, J. J.; Dapprich, S.; Daniels, A. D.; Farkas, Ö.; Foresman, J. B.; Ortiz, J. V.; Cioslowski, J.; Fox, D. J. *Gaussian 09*, Gaussian, Inc.: Wallingford, CT, USA, 2009.
5. Joung, I. S.; Cheatham, T. E., Determination of Alkali and Halide Monovalent Ion Parameters for Use in Explicitly Solvated Biomolecular Simulations. *J. Phys. Chem. B* **2008**, *112* (30), 9020-9041.
6. Martínez, L.; Andrade, R.; Birgin, E. G.; Martínez, J. M., PACKMOL: A Package for Building Initial Configurations for Molecular Dynamics Simulations. *J. Comput. Chem.* **2009**, *30*, 2157-2164.
7. Qiao, B.; Demars, T.; Olvera de la Cruz, M.; Ellis, R. J., How Hydrogen Bonds Affect the Growth of Reverse Micelles around Coordinating Metal Ions. *J. Phys. Chem. Lett.* **2014**, *5* (8), 1440-1444.
8. Darden, T.; York, D.; Pedersen, L., Particle Mesh Ewald: An  $N \log(N)$  Method for Ewald Sums in Large Systems. *J. Chem. Phys.* **1993**, *98*, 10089-92.
9. Essmann, U.; Perera, L.; Berkowitz, M. L.; Darden, T.; Lee, H.; Pedersen, L., A Smooth Particle Mesh Ewald Method. *J. Chem. Phys.* **1995**, *103*, 8577-93.
10. Eicke, H. F.; Christen, H., Nucleation process of micelle formation in apolar solvents. *J. Colloid Interface Sci.* **1974**, *48*, 281-90.
11. Eicke, H. F.; Shepherd, J. C. W.; Steinemann, A., Exchange of solubilized water and aqueous electrolyte solutions between micelles in apolar media. *J. Colloid Interface Sci.* **1976**, *56*, 168-76.
12. Atik, S. S.; Thomas, J. K., Transport of ions between water pools in alkanes. *Chem. Phys. Lett.* **1981**, *79*, 351-4.
13. Rees, G. D.; Robinson, B. H., Microemulsions and organogels: properties and novel applications. *Adv. Mater. (Weinheim, Fed. Repub. Ger.)* **1993**, *5*, 608-19.
14. Pileni, M.-P., The role of soft colloidal templates in controlling the size and shape of inorganic nanocrystals. *Nat. Mater.* **2003**, *2*, 145-150.
15. Levinger, N. E., Perspectives. Chemistry. Water in confinement. *Science (Washington, DC, U. S.)* **2002**, *298*, 1722-1723.
16. Yagmur, A.; Glatter, O., Characterization and potential applications of nanostructured

- aqueous dispersions. *Adv. Colloid Interface Sci.* **2009**, *147-148*, 333-342.
17. Baruah, B.; Roden, J. M.; Sedgwick, M.; Correa, N. M.; Crans, D. C.; Levinger, N. E., When is water not water? Exploring water confined in large reverse micelles using a highly charged inorganic molecular probe. *J. Am. Chem. Soc.* **2006**, *128*, 12758-65.
  18. Piletic, I. R.; Moilanen, D. E.; Spry, D. B.; Levinger, N. E.; Fayer, M. D., Testing the Core/Shell Model of Nanoconfined Water in Reverse Micelles Using Linear and Nonlinear IR Spectroscopy. *J. Phys. Chem. A* **2006**, *110*, 4985-4999.
  19. Fayer, M. D.; Levinger, N. E., Analysis of water in confined geometries and at interfaces. *Annu. Rev. Anal. Chem.* **2010**, *3*, 89-107.
  20. Giustini, M.; Palazzo, G.; Colafemmina, G.; Della Monica, M.; Giomini, M.; Ceglie, A., Microstructure and Dynamics of the Water-in-Oil CTAB/n-Pentanol/n-Hexane/Water Microemulsion: A Spectroscopic and Conductivity Study. *J. Phys. Chem.* **1996**, *100* (8), 3190-3198.
  21. Humphrey, W.; Dalke, A.; Schulten, K., VMD: Visual Molecular Dynamics. *J. Mol. Graphics* **1996**, *14*, 33-38.
  22. Fritz, G.; Bergmann, A.; Glatter, O., Evaluation of small-angle scattering data of charged particles using the generalized indirect Fourier transformation technique. *J. Chem. Phys.* **2000**, *113*, 9733-9740.
  23. Glatter, O., The interpretation of real-space information from small-angle scattering experiments. *J. Appl. Crystallogr.* **1979**, *12*, 166-175.
  24. Aswal, V. K.; Goyal, P. S.; Amenitsch, H.; Bernstorff, S., Counterion condensation in ionic micelles as studied by a combined use of SANS and SAXS. *Pramana* **2004**, *63*, 333-338.